ISSN: 2447-3359

REVISTA DE GEOCIÊNCIAS DO NORDESTE

Northeast Geosciences Journal

v. 11, nº 1 (2025)

https://doi.org/10.21680/2447-3359.2025v11n1ID37740

Mineralogical analysis and technological applications of the residue from extraction of emeralds from the Carnaíba and Socotó/BA mines in ceramic mass composition

Análise mineralógica e aplicações tecnológicas do resíduo da extração de esmeraldas dos Garimpos de Carnaíba e Socotó/BA em composição de massas cerâmicas

Talita Fernanda Carvalho Gentil[1]; José de Araújo Nogueira Neto[2]; Irani Clezar Mattos[3]; Martha Noélia Lima[4]; Tércio Graciano Machado[5]; Vinícius Ferraz Guimarães[6]

[1] Federal University of Ceará, Graduate Program in Geology, Fortaleza/CE, Brazil. Email: tfernanda.gentil@gmail.com
Federal Institute of Bahia, Jacobina Campus, Jacobina/BA, Brazil. Email: talita.gentil@ifba.edu.br
ORCID: https://orcid.org/0000-0002-5019-5171

[2] Federal University of Ceará, Graduate Program in Geology, Fortaleza/CE, Brazil. Email: nogueira@ufc.br
Federal University of Goiás, Faculty of Science and Technology, Goiânia/GO, Brazil. Email: jose.araujo@ufg.br
ORCID: https://orcid.org/0000-0003-3706-2443

[3] Federal University of Ceará, Department of Geology, Fortaleza/CE, Brazil. Email: irani.mattos@ufc.br
ORCID: https://orcid.org/0000-0002-5971-4433

[4] Federal University of Ceará, Department of Mining Engineering, Crateús/CE, Brazil. Email: martha.lima@crateus.ufc.br
ORCID: https://orcid.org/0000-0003-4762-5502

[5] Federal Institute of Bahia, Jacobina Campus, Jacobina/BA, Brazil. Email: gracianomil@hotmail.com
ORCID: https://orcid.org/0000-0003-2764-3316

[6] Federal University of Goiás, Faculty of Science and Technology, Goiânia/GO, Brazil. Email: viniciusfg@ufg.br
ORCID: https://orcid.org/0009-0002-0555-4881

Abstract: The extraction of emeralds in the Carnaíba and Campo Formoso mountain ranges in Bahia generates significant environmental residue. This study aimed to characterize the residue from the Carnaíba (Pindobaçu-BA) and Socotó (Campo Formoso-BA) mines and to develop composite materials with clay for the production of ceramic materials in the construction industry. Formulations were prepared with varying concentrations of clay and mineral residue (10%, 20%, 30%, 40%, and 50%), which were subjected to chemical and mineralogical analyses using X-ray fluorescence and diffraction. The samples were sintered at different temperatures (850°C, 900°C, 950°C, 1000°C, 1100°C, and 1200°C) and tested for water absorption (WA%), apparent porosity (AP%), linear shrinkage (LS%), loss on ignition (LOI%) and flexural strength (FS MPa). The results revealed important characteristics for the ceramic industry, such as the presence of SiO_2 and Al_2O_3, which positively affect the properties of the final pieces. The mineralogical diversity, including mullite, metakaolinite, indialite, and quartz, contributed to the strength and stability of the composites. The formulations C_{20} (20% Carnaíba residue) and S_{10} (10% Socotó residue) achieved the best results, standing out for their technical feasibility and sustainability in ceramic production.

Keywords: Mineral Reuse; Sustainability; Mechanical Properties.

Resumo: A exploração de esmeraldas nas Serras da Carnaíba e de Campo Formoso, na Bahia, gera significativos resíduos ambientais. Este estudo teve como objetivo caracterizar os resíduos dos garimpos de Carnaíba (Pindobaçu-BA) e Socotó (Campo Formoso-BA) e desenvolver materiais compostos com argila para a produção de materiais cerâmicos na construção civil. Foram elaboradas formulações com concentrações de argila e resíduos minerais variando entre 10%, 20%, 30%, 40% e 50 %, as quais foram submetidas a análises químicas e mineralógicas por meio de fluorescência e difração de raios - X. As amostras foram sinterizadas em diferentes temperaturas (850ºC, 900ºC, 950ºC, 1000ºC, 1100ºC e 1200ºC) e submetidas a ensaios tecnológicos de absorção de água (AA %), porosidade aparente (PA%), retração linear (RL%), perda ao fogo (PF%) e resistência à flexão (RF MPa). Os resultados revelaram características importantes para a indústria cerâmica, como a presença da SiO_2 e Al_2O_3, que afetam, favoravelmente, as propriedades das peças. A diversidade mineralógica, incluindo mulita, metacaulinita, indialita e quartzo, contribuiu para a resistência e estabilidade dos compósitos. As formulações C_{20} (20 % de resíduo de Carnaíba) e S_{10} (10 % de resíduo de Socotó) apresentaram os melhores resultados, destacando-se pela viabilidade técnica e sustentabilidade na produção cerâmica.

Palavras-chave: Reutilização Mineral; Sustentabilidade; Propriedades Mecânicas.

Received: 20/09/2024; Accepted: 11/03/2025; Published: 20/03/2025.

1. Introduction

The construction industry has always been one of the largest consumers of natural resources, playing a significant role in environmental impact and the demand for raw materials. In this context, the advancement of alternative materials for this sector becomes evident, aiming to reduce costs, minimize environmental impacts, and incorporate solid residues. Within this scenario, Silveira (2015) highlights the relevance of using residues from mining activities due to the substantial production volume and the considerable amount of residues generated throughout all stages of this industry's production process.

The extraction of emeralds in the northeastern region of the state of Bahia, particularly in the Jacobina Mountain Range, results in the production of substantial volumes of emerald residue, which is often discarded into the environment. The main mineral constituents present in these residues include micas (phlogopite, biotite), quartz, and molybdenite. A trend observed in recent years is the growing interest in using these mineral residues as additives in the manufacturing of ceramic materials (BERGMAN, 2016; SILVA, 2018; JÚNIOR, 2022), aiming to improve product quality and expand its possible applications.

The extraction and processing of emeralds in the Carnaíba and Socotó mines cause various socio-environmental impacts. In this context, the unregulated exploitation of these areas is particularly noteworthy, as they lack prior studies and specialized techniques, as indicated by Cavalcante (2010). Among these impacts, the indiscriminate accumulation of residues, randomly disposed of in the environment, stands out, as documented by Braga (2013).

This study proposes an in-depth analysis of the technical feasibility of using residues resulting from the unregulated extraction of emeralds in the Carnaíba (Pindobaçu – BA) and Socotó (Campo Formoso – BA) mines (as shown in Figure 1) as an alternative raw material for the production of ceramic materials. The focus will be on formulating ceramic composites with different concentrations of emerald residues, ranging from 10% to 50%. This study aims not only to assess technical feasibility but also to highlight the potential of incorporating these residues into the ceramic industry, promoting a more sustainable and innovative approach.

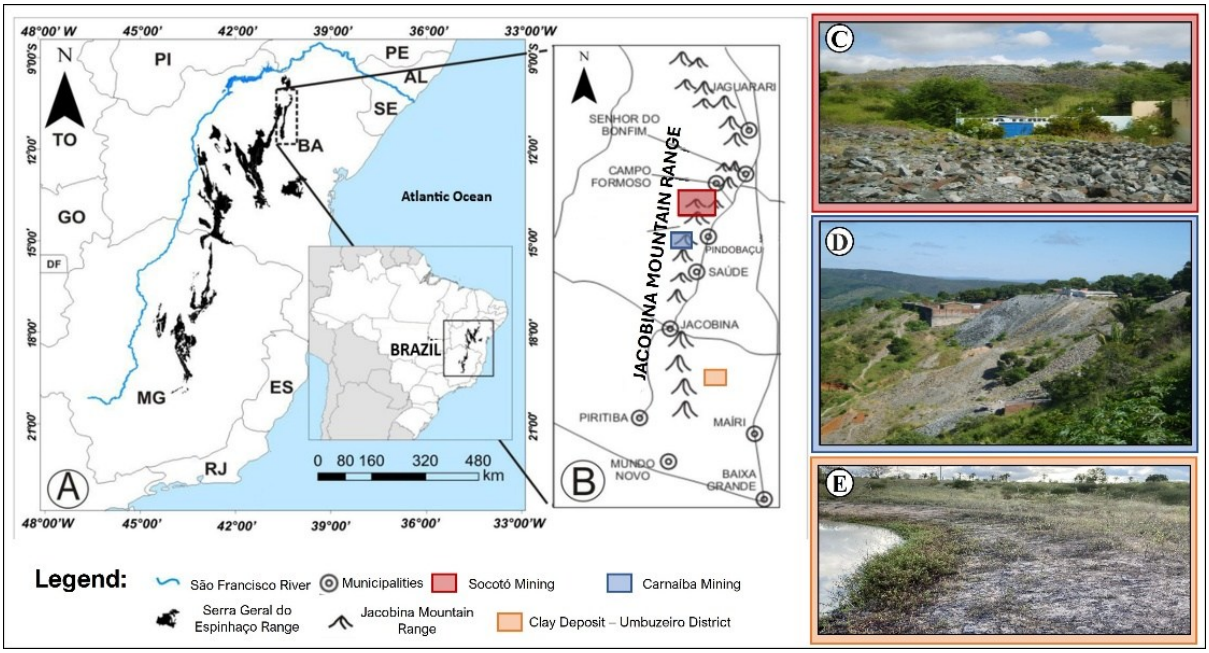

Figure 1 – Geographical location map of the study areas (A) within the Serra da Jacobina (B) and images of the Socotó mining site (C), Carnaíba mining site (D), and the Clay Deposit at Faz. Caldeirão da Errata in the Umbuzeiro District (E).

Source: Maps adapted from IBGE (2007); CPRM (2010) and images by the authors (2024).

2. Methodology

In this study, ten ceramic formulations were prepared with up to 50% by weight of emerald extraction residue, as shown in Table 1.

Table 1 – Composition and nomenclature of the formulations.

Formulations	Composition	
	Clay (%)	Residue (%)
A	100	0
C	0	100
C_{10}	90	10
C_{20}	80	20
C_{30}	70	30
C_{40}	60	40
C_{50}	50	50
S	0	100
S_{10}	90	10
S_{20}	80	20
S_{30}	70	30
S_{40}	60	40
S_{50}	50	50

Source: Authors (2024).
A: Clay. C: Carnaíba Mining Residue. S: Socotó Mining Residue.

For the preparation of the ceramic masses, clay obtained from a deposit located in the Umbuzeiro-BA district and residues from the Carnaíba and Socotó mines were used. The clay and residue samples were dried in an oven at 110°C for 24 hours, then fragmented, ground, and sieved with a 74 μm mesh (ABNT 200 sieve).

The raw materials were ground and properly homogenized, and aliquots were taken for chemical and mineralogical analyses. The chemical analysis was performed using X-ray fluorescence (XRF) with a Bruker S8 Tiger WDS spectrometer, while the mineralogical analysis was conducted using X-ray diffraction (XRD) with a Bruker D8 Discover diffractometer. The samples were analyzed before and after the firing stage.

The quantification of major elements was carried out using Bruker's GeoQuant M® package, employing natural rock and mineral standards. The quantification of molybdenum oxide was performed using Bruker's semi-quantitative Quant-Express® package. For minor elements, the GeoQuant T® calibration curve package from Bruker was used, with results expressed in parts per million (ppm).

The mineralogical analysis was conducted using monochromatic radiation provided by a copper anode tube, coupled with a Johansson monochromator for Kα1, operating at 40 kV and 40 mA. The configuration used was Bragg-Brentano θ-2θ, with a Lynxeye® detector, covering a 2θ range from 3° to 100° with a step size of 0.01°. The identification of crystalline phases was performed using the X'Pert HighScore software, which compares the obtained diffractogram peaks with PDF2 standards, allowing for the determination of the phases present in the samples.

In addition to chemical and mineralogical analyses, elemental sulfur and carbon analyses were also conducted on the samples to assess how these elements influence the behavior of the ceramic masses during firing. Sulfur can cause defects, while carbon affects porosity and coloration. These data are essential for optimizing firing conditions and ensuring material quality.

To obtain test specimens for analyzing ceramic properties, the formulations described in Table 1 were prepared and homogenized in a ball mill for 15 minutes, then moistened with 10% distilled water to acquire plasticity, facilitating the subsequent compaction stage of the test specimens.

The shaping of the test specimens was performed using a metallic mold (60 mm × 20 mm × 6 mm) with a Bonevau hydraulic press (15 tons) at a pressure of 5 MPa. After shaping, the specimens were subjected to drying in an electric oven at 110°C for 24 hours to ensure complete removal of residual moisture.

The sintering of the test specimens was carried out in a Quimis muffle furnace, following a thermal cycle with a 1-hour isothermal stage at temperatures of 850°C, 900°C, 950°C, 1000°C, 1100°C, and 1200°C, with a heating rate of 10°C/min. After the isothermal stage, the furnace was turned off, and the specimens were subjected to natural cooling inside the furnace until reaching room temperature.

With the test specimens produced, technological tests were conducted, whose details, including the mathematical formulas used, are presented in Table 2.

Table 2 – Technological tests and their respective mathematical formulas applied to the studied samples.

Technological Tests	Linear Firing Shrinkage (%)	Water Absorption (%)	Apparent Porosity (%)	Flexural Strength (MPa)
Formulas	LFS = (Cs-Cq/Cs) x 100	WA = (Mu-Ms/Ms) x 100	AP = (Mu-Ms/Mu-Mi) x 100	FS = 3.F.L/2.b.h^2

Source: Authors (2024).

In addition to the analyses performed in this study, gresification tests were carried out to evaluate the densification of the ceramic formulations as a function of firing temperature, assessing water absorption, linear shrinkage, and porosity. These parameters are essential for understanding sample compaction, allowing their suitability for different ceramic applications, aiming for properties such as mechanical strength and low porosity.

3. Results and Discussion

Table 3 presents the results of the chemical analysis of the raw materials. In the analysis of the clay (A), silicon oxide (SiO_2) has the highest percentage among the elements, followed by aluminum oxide (Al_2O_3) and iron oxide (Fe_2O_3). These results indicate the potential of this clay for producing high-quality ceramic materials (PRADO, 2011; VIEIRA *et al*., 2007). Fluxing oxides (K_2O, Na_2O, CaO, and MgO) are also detected in low concentrations, with a total sum of 2.15%.

Table 3 – Chemical composition of the studied raw materials.

Oxides	**SiO_2**	**Al_2O_3**	**Fe_2O_3**	**TiO_2**	**MnO**	**MgO**	**CaO**	**Na_2O**	**K_2O**	**P_2O_5**	**MoO_3***	**LOI**	**Total**
Samples	Weight %												
A	54.29	28.34	4.35	0.63	<LQ	0.50	<LQ	0.36	1.29	<LQ	<LQ	10.86	100.62
C	34.98	11.65	4.28	0.17	0.11	11.99	13.62	0.16	3.87	9.93	6.40	3.64	100.80
S	47.09	9.71	8.70	0.22	0.14	23.59	2.24	0.25	4.82	<LQ	<LQ	4.12	100.89

Source: Authors (2024).
(<LQ): Below the quantifiable limit. (*): Semi-quantitative result.
A: Clay. C: Carnaíba Mining Residue. S: Socotó Mining Residue.

The analyzed clay showed a loss on ignition (LOI) of 10.86%, which is directly related to the concentration of aluminum (Al) present in the sample. This loss on ignition primarily refers to the amount of water released during the firing process, resulting from the dehydroxylation of hydroxyl (-OH) groups in clay minerals such as kaolinite (MORENO *et al*., 2016). When these -OH groups are heated, they decompose and release water in the form of vapor, contributing to the reduction in sample mass, which reflects the mineralogical composition and thermal stability of the clay.

In the residue samples from the Carnaíba (C) and Socotó (S) mines, the predominance of silicon oxide (SiO_2) and aluminum oxide (Al_2O_3) is observed. However, the concentrations of fluxing oxides are higher in these raw materials, reaching 29.64% in sample C and 30.90% in sample S.

The amount of fluxing oxides present in the raw materials was highest in sample S, which is important for the synthesis process of mullite ($3Al_2O_3{\cdot}2SiO_2$), as these oxides promote diffusion through the formation of a liquid phase.

The material with the highest alumina/silica ratio is sample S (4.85), while the clay sample (A) had the lowest ratio (2.09). This parameter is particularly significant for the mullite formation process ($3Al_2O_3{\cdot}2SiO_2$).

The significant presence of Fe_2O_3 in the studied samples is a determining factor for the reddish coloration observed after the firing process. The raw material with the highest iron oxide content is sample S (8.70%), while the material with the lowest percentage of this oxide is found in sample C (4.28%). Iron (Fe_2O_3), titanium (TiO_2), calcium (CaO), and magnesium (MgO) oxides are frequently associated with the red coloration of ceramics after firing (PRADO, 2011).

In sample C, which incorporates residue from the Carnaíba mine, the presence of phosphorus oxide (P_2O_5) at approximately 9.93% and molybdenum oxide (MoO_3) at around 6.4% is observed, indicating a considerable concentration of these compounds. At high firing temperatures, P_2O_5, in combination with silica (SiO_2), can act as a flux and opacifier, functioning as a glass former (IRVINE; MURPHY, 2018; KANG, 2004; SCHROEDER; KALIDINDI, 2023; SOKHANVAR; SADEGHI, 2020).

Molybdenum oxide, on the other hand, is described in the literature as a reducing agent in ceramic bodies rather than a flux or stabilizer (BURCH, 1978; KUMAR; PATEL, 2022). During the firing process, MoO_3 can react with other oxides, promoting the reduction of ceramic pieces and potentially influencing the formation of specific mineral phases, as evidenced in the X-ray diffraction analyses.

Table 4 presents the results of the elemental sulfur and carbon analyses performed on the raw materials used in the ceramic mass composition, highlighting their means, standard deviations, and relative percentage variations (%RSD).

Table 4 – Results of sulfur and elemental carbon analyses of the raw materials.

Samples	Sulfur (M)	Sulfur (DP)	Sulfur (% RSD)	Carbon (M)	Carbon (DP)	Carbon (%RSD)
A	0.02%	0.01%	22.3	0.72%	0.00%	0.115
C	3.82%	0.16%	4.26	0.14%	0.00%	1.75
S	0.02%	0.02%	127	0.31%	0.00%	0.985

Source: Authors (2024).
M: Mean. SD: Standard Deviation. %RSD: Relative Standard Deviation.

The sulfur and carbon analyses of the raw materials reveal significant variations between the materials. The Carnaíba residue exhibited the highest sulfur content (3.82%) with low variability (%RSD of 4.26), while the Socotó residue and clay showed very low sulfur concentrations (0.02%), with the Socotó residue displaying higher variability (%RSD of 127). Regarding carbon, clay exhibited the highest content (0.72%), followed by the Socotó residue (0.31%) and the Carnaíba residue (0.14%), all with low variability, as indicated by the low %RSD values. These results provide an accurate insight into the elemental composition of the samples.

In the mineralogical analysis of the clay, presented in Figure 2, the predominance of quartz (SiO_2) and kaolinite ($Al_2Si_2O_5(OH)_4$) is notable, along with the presence of microcline ($KAlSi_3O_8$) and muscovite ($Kal_2(AlSi_3O_{10})(OH)_2$).

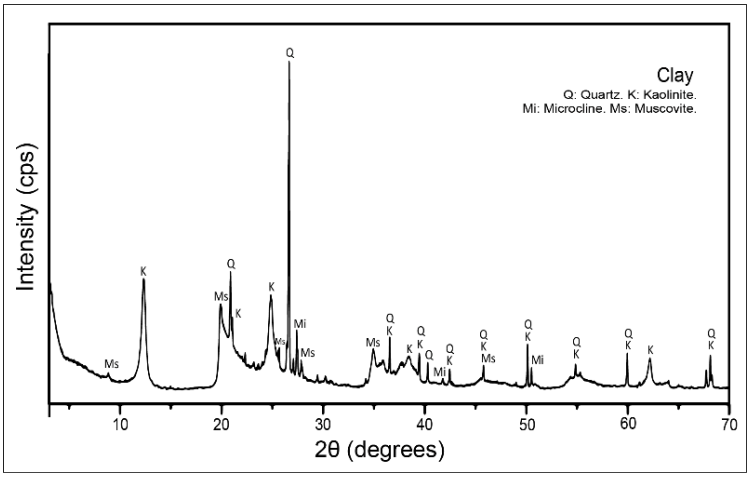

Figure 2 – X-ray diffraction patterns of clay.
Source: Authors (2024).

In the diffractogram, the presence of silica (SiO_2) was observed along with the mineral phases quartz, kaolinite, microcline, and muscovite, which is consistent with the results of the chemical analysis, as silicon from these phases was accounted for. Microcline is identified as a potassium and aluminum silicate, elements detected in the X-ray fluorescence analysis. Kaolinite is recognized by peaks around 12.4° and 24.8° (2θ), corresponding to its lamellar structure, composed

of alternating layers of aluminum octahedra and silica tetrahedra. Meanwhile, muscovite exhibits a prominent peak around 8.8° (2θ), related to the spacing between its silicate layers. The presence of these peaks is essential for confirming the mineralogical composition in ceramic mixtures, in conjunction with data from chemical and thermal analyses (ACEVEDO *et al*., 2017; MACEDO *et al*., 2008; SANTOS, 1989).

The diffractograms presented in Figure 3 reveal the mineralogical composition of the emerald residue samples from the Carnaíba and Socotó mines.

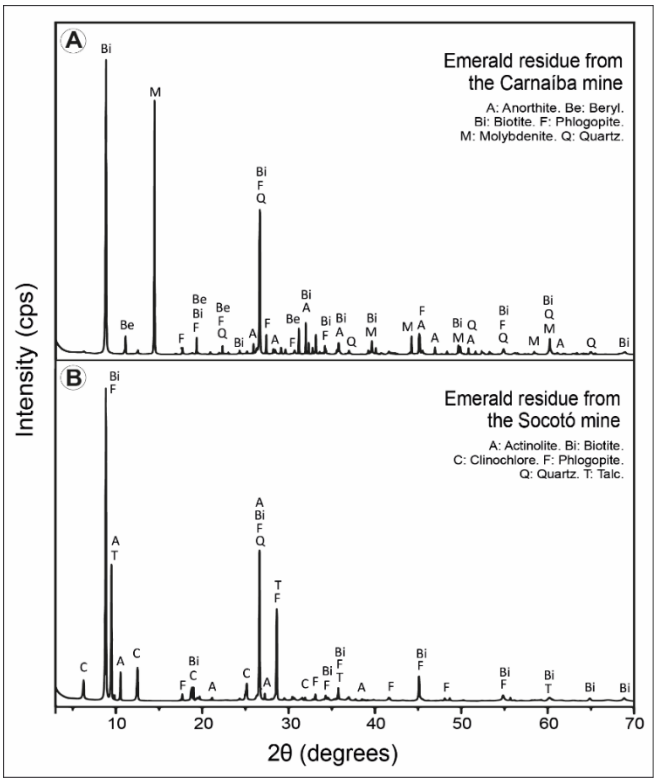

Figure 3 – X-ray diffraction patterns of emerald mining residues. A) Carnaíba mining site; B) Socotó mining site. Source: Authors (2024).

The high iron contents found in the chemical composition of these samples are associated with the presence of the mineral biotite ($K(Mg,Fe)_3(AlSi_3O_{10})(OH,F)_2$). Phlogopite, whose chemical composition is described as ($KMg_3(AlSi_3O_{10})(F,OH)_2$), is also identified in multiple phases of the analyzed diffractograms. In the sample containing mineral residue from the Carnaíba mine, the significant presence of the mineral molybdenite (MoS_2) stands out, which is consistent with the high molybdenum oxide (MoO_3) contents determined for this sample. Other identified minerals include quartz (SiO_2), anorthite ($CaAl_2Si_2O_8$), actinolite ($Ca_2(Mg,Fe)_5Si_8O_{22}(OH)_2$), beryl ($Be_3Al_2Si_6O_{18}$), talc ($Mg_3Si_4O_{10}(OH)_2$), and clinochlore ($Mg_5Al(AlSi_3)O_{10}(OH)_8$), all belonging to the silicate group. The chemical composition of these minerals is consistent with the data obtained through X-ray fluorescence, indicating a significant presence of calcium, aluminum, iron, and magnesium. These results align with the data presented by Silva *et al*. (2021) and Vieira *et al*. (2007) in their studies on the inclusion of mineral residues in ceramic masses.

In Figure 4, the linear shrinkage values of the test specimens after firing at 850°C, 900°C, 950°C, 1000°C, 1100°C, and 1200°C are observed. The data analysis reveals a progressive increase in linear shrinkage with the rise in firing temperature, especially above 1000°C, except in formulations C_{30}, C_{40}, and C_{50}, where sample melting occurred.

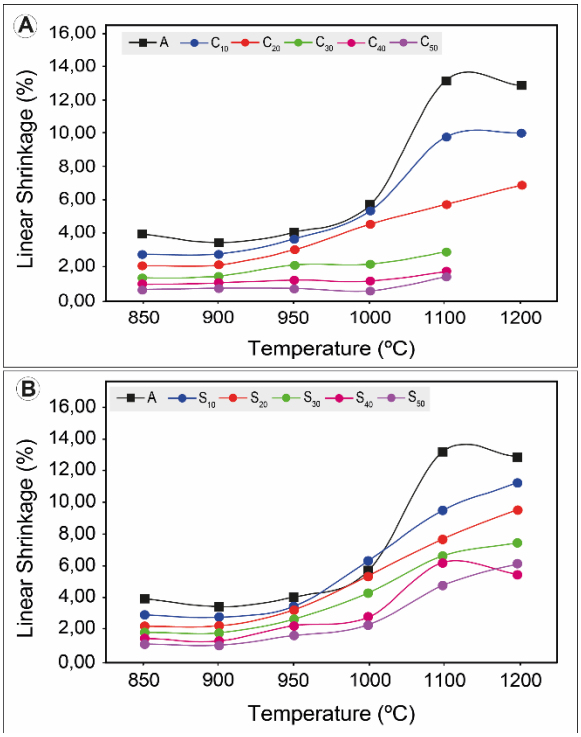

Figure 4 – Results of the linear shrinkage test for the formulations. A: Clay. C: Carnaíba Mining Residue. S: Socotó Mining Residue. Source: Authors (2024).

The melting of ceramic mass samples containing 30% to 50% emerald mineral residue at 1200°C occurs due to the proximity of this temperature to the boiling point of lithium (1300°C), which is found in abundance in basement rocks (COSTA, 2019). However, it is important to note that lithium is not detected in X-ray fluorescence (XRF) analyses, as it is a light element, which prevents its identification using this technique. The presence of water in the mineral structure causes a reduction in the melting temperature since it alters the crystalline structure of the materials (MARSCHNER, 2011). This effect is more evident in samples with a higher content of Carnaíba residue and higher moisture content, as observed in the linear shrinkage and water absorption tests.

In formulations C and S, which contain between 10% and 20% emerald residue, a sharp reduction in shrinkage was observed from 1100°C compared to the sample containing 100% clay. This behavior can be attributed to the dense packing of particles during shaping, which, when heated, favored the formation of a liquid phase, promoting sintering and resulting in greater shrinkage of the pieces.

On the other hand, in formulations C and S with emerald residue contents above 30%, a slight expansion was observed starting at 900°C. This expansion is attributed to the presence of mica-group minerals, such as biotite and phlogopite, in the ceramic mass. The addition of more than 30% emerald residue to the ceramic mass increased the mica percentage, and, as reported in the literature (MENEZES *et al*., 2006; MORENO *et al*., 2016), ceramic masses containing mica and subjected to temperatures between 600°C and 900°C exhibit expansion due to mica dehydroxylation.

The results of the samples produced with the C_{20} formulation align with the data obtained by Cavalcante *et al*. (2012), who investigated the incorporation of emerald mining residue into ceramic masses for coatings. This study demonstrates that the addition of mineral residues from emerald mining can positively influence the properties of ceramic masses, such as strength and thermal stability, reinforcing the feasibility of using these materials in the ceramic sector.

In Figure 5, the water absorption values (Figures 5A and 5B) and apparent porosity values (Figures 5C and 5D) for both clay and formulations C and S are shown. These values are consistent with the results of the linear shrinkage tests discussed earlier. It is noted that as the temperature increases up to 1200°C, all formulations exhibit a reduction in water absorption and apparent porosity, which can be explained by the presence of fluxing oxides, such as Fe_2O_3 and K_2O, in the chemical composition of the clay and formulations. According to Babisk *et al*. (2012) and Moreno *et al*. (2016), samples

containing Fe and K oxides, when exposed to high temperatures, undergo fusion and can fill the empty pores present in the samples.

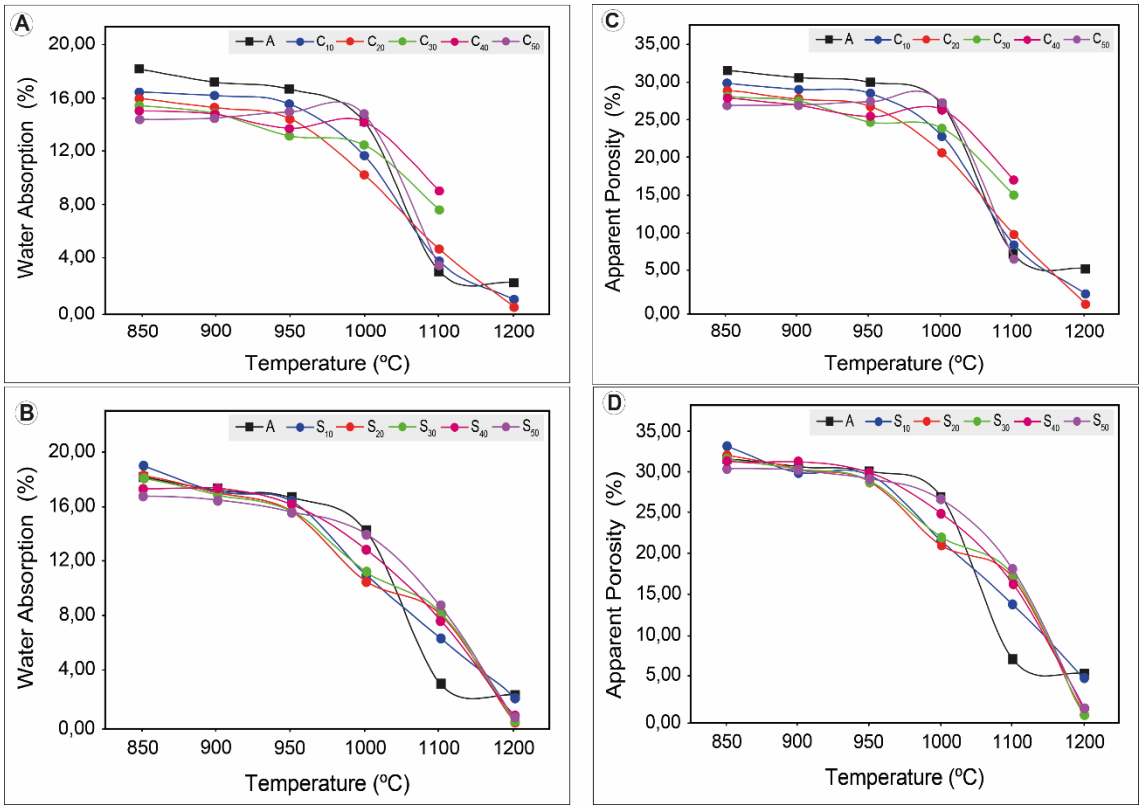

Figure 5 – Results of the water absorption and apparent porosity test for the formulations. A: Clay. C: Carnaíba Mining Residue. S: Socotó Mining Residue. Source: Authors (2024).

The most significant reductions in water absorption and apparent porosity were recorded from 1100°C in clay and in formulations C_{10}, C_{20}, and S_{10}, with mineral residue contents ranging from 0% to 20%, with water absorption values between 2.9% and 6.3% and apparent porosity values between 6.59% and 13.79%. Meanwhile, the minimum water absorption and apparent porosity at 1200°C were observed in formulations C and S, with residue contents ranging from 10% to 50%, oscillating between 4.82% and 0%.

Figure 6 shows the results of the three-point bending strength test performed on the clay and the studied formulations, along with their respective standard deviations at different firing temperatures.

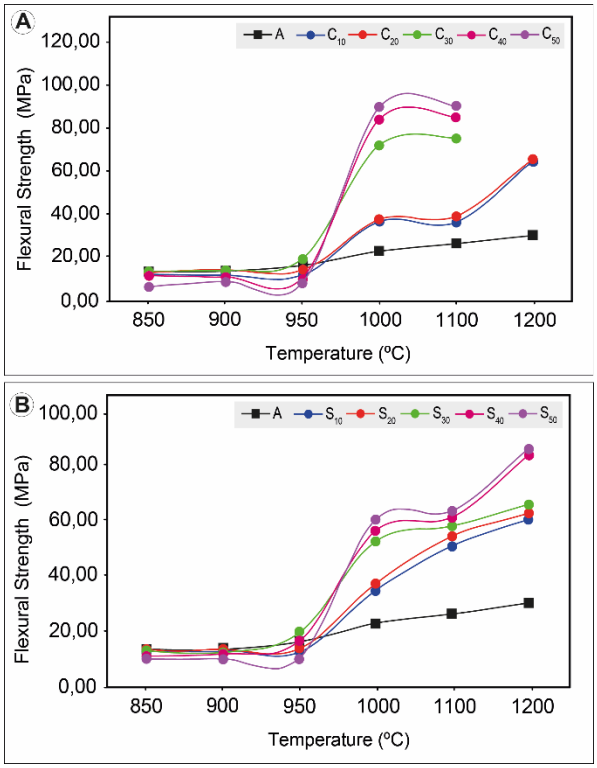

Figure 6 – Results of the three-point flexural strength test for the formulations. A: Clay. C: Carnaíba Mining Residue. S: Socotó Mining Residue. Source: Authors (2024).

The three-point bending strength results for the clay and the studied formulations indicate that the higher the firing temperature, the greater the strength. The mechanical properties of the ceramic piece result from denser particle organization, the formation of new phases, and greater compaction. These factors enhance the bonding strength between particles, providing greater material resistance.

At temperatures of 850°C and 950°C, the ceramic pieces obtained from formulations containing mineral residue showed lower strength. The presence of quartz in the clay and formulations may impact the behavior of ceramic pieces during cooling after thermal treatment. This occurs because quartz undergoes changes in its crystalline structure (structural transformations) when heated and cooled. These changes can generate internal stresses in the material, leading to cracks. Cracks, in turn, concentrate these stresses, which can compromise the integrity and strength of the final material.

When analyzing the temperature of 1000°C, a significant increase in strength was observed in all test specimens, particularly in formulations containing residue. However, at 1100°C, a decreasing trend in strength was observed only in formulations C and S, followed by a renewed increase in strength at 1200°C.

Among the formulations analyzed in this study, formulations C_{20} and S_{10} stood out for presenting the most appropriate and consistent results. These formulations were characterized based on the thermal evolution of the mineralogical composition, the gresification analysis, and the obtained bending strength results. The combination of these factors demonstrates the effectiveness of the formulations in terms of mechanical performance and thermal stability, making them the most suitable for this study.

In the diffractogram shown in Figure 7, for the C_{20} formulation (natural/unfired), the presence of the following mineral phases is observed: molybdenite (MoS_2), kaolinite ($Al_2Si_2O_5(OH)_4$), phlogopite ($KMg_3(AlSi_3O_{10})(F,OH)_2$), biotite ($K(Mg,Fe)_3(AlSi_3O_{10})(OH,F)_2$), quartz ($SiO_2$), and beryl ($Be_3Al_2Si_6O_{18}$).

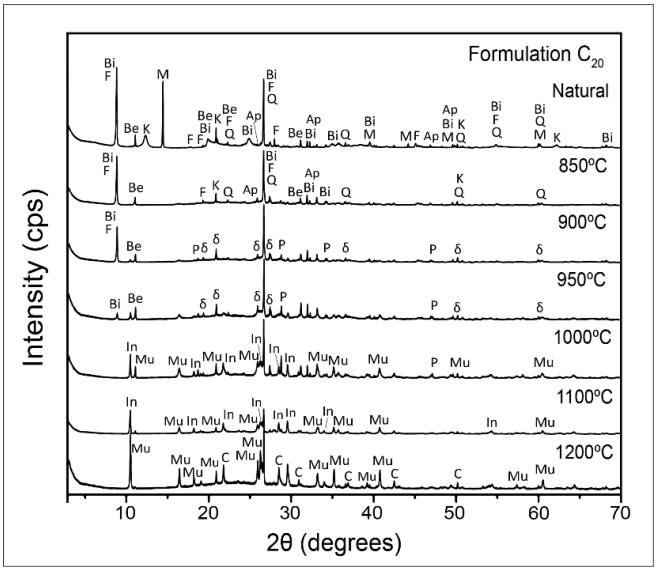

Figure 7 – X-ray diffraction pattern showing the thermal evolution of the C_{20} formulation before and after firing. Identified crystalline phases: Q: Quartz. M: Molybdenite. K: Kaolinite. Mu: Mullite. Bi: Biotite. F: Phlogopite. Be: Beryl. δ: Metakaolinite. P: Powellite. In: Indialite. C: Cristobalite.
Source: Authors (2024).

The thermal evolution of the C_{20} formulation reveals that, as the temperature increases, significant transformations occur in the mineral phases. Between 850°C and 900°C, molybdenite begins to oxidize, forming molybdenum trioxide (MoO_3), while kaolinite dehydroxylates to form metakaolinite ($Al_2Si_2O_7$). The formation of powellite ($CaMoO_4$) at 900°C indicates that the temperature conditions are sufficient to initiate a reaction between the components present in the sample, specifically molybdenum trioxide (MoO_3), resulting from the oxidation of molybdenite (MoS_2), and calcium, possibly originating from anorthite ($CaAl_2Si_2O_8$) present in the residue from the Carnaíba mine.

As reported by Cavalcante *et al*. (2012), anorthite was not detected in the formulations analyzed in their study, a result that is repeated in the present research, even in formulations with 50% residue. This result reinforces the data obtained by Cavalcante *et al*. (2012), indicating that during the firing process, reactions occurred between the emerald residue and the clay, the main components of the ceramic formulations investigated.

Between 950°C and 1000°C, the oxidation of molybdenite continues, and metakaolinite begins to transform into mullite ($3Al_2O_3{\cdot}2SiO_2$). Micas (phlogopite and biotite) may form additional phases, such as enstatite and other pyroxenes. Powellite remains stable but may begin to decompose at higher temperatures.

In the range of 1000°C to 1100°C, mullite formation from kaolinite intensifies, and quartz begins its transformation into cristobalite.

Between 1100°C and 1200°C, mullite becomes more stable, while indications suggest the presence of amorphous silica, possibly derived from kaolinite residues. As beryl decomposes, it contributes BeO and Al_2O_3 to the formation of complex phases, potentially influencing mullite formation. Indialite (the hexagonal form of cordierite) may form from magnesium, aluminum, and silica-rich phases at temperatures above 1100°C (LIMA *et al*., 1998). Cristobalite remains present as one of the high-temperature phases of quartz. These transformations indicate a complex interaction between the present minerals, resulting in the formation of new stable mineral phases at high temperatures.

Figure 8 shows the diffractogram of the S_{10} formulation in its natural state, highlighting the presence of the mineral phases quartz (SiO_2), muscovite ($Kal_2(AlSi_3O_{10})(OH)_2$), microcline ($KAlSi_3O_8$), phlogopite ($KMg_3AlSi_3O_{10}(OH)_2$), talc ($Mg_3Si_4O_{10}(OH)_2$), and kaolinite ($Al_2Si_2O_5(OH)_4$), as confirmed by the chemical analysis of the predominant oxides.

Phlogopite exhibits main peaks around 8.4° and 26.5° (2θ), which are associated with its phyllosilicate crystalline structure, characterized by alternating layers of silica tetrahedra and octahedra containing magnesium and iron. Talc, in turn, is identified by a peak at approximately 28.6° (2θ), indicating its lamellar structure composed of layers of silica tetrahedra and magnesium octahedra, as detailed in the study by Yin, Zhu, and Zeng (2010).

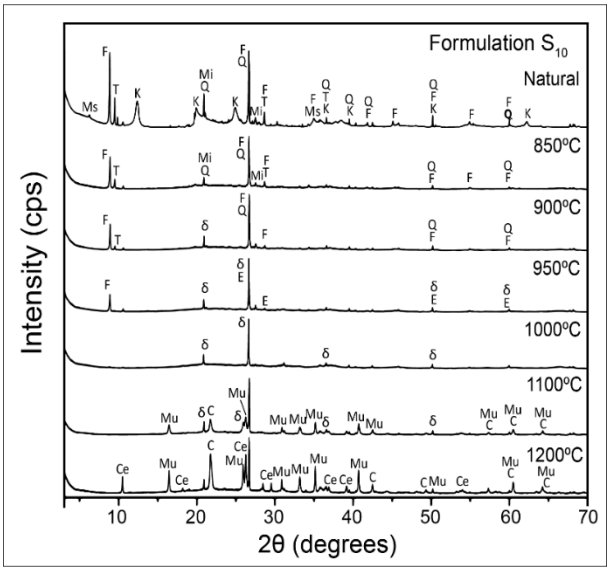

Figure 8 – X-ray diffraction pattern showing the thermal evolution of the S_{10} formulation before and after firing. Identified crystalline phases: Q: Quartz. Mi: Microcline. Ms: Muscovite. K: Kaolinite. Mu: Mullite. F: Phlogopite. T: Talc. δ: Metakaolinite. E: Enstatite. Ce: Clinoenstatite. C: Cristobalite.
Source: Authors (2024).

The thermal evolution of the S_{10} formulation confirms that between 850°C and 950°C, kaolinite undergoes dehydroxylation to form metakaolinite ($Al_2Si_2O_5(OH)_4 \rightarrow Al_2Si_2O_7 + 2H_2O$), resulting in an amorphous phase with no defined structure, as reported by Santos *et al*. (2013) and Menshaz *et al*. (2017). Talc heated in this temperature range dehydroxylates to form enstatite and amorphous silica through the reaction ($Mg_3Si_4O_{10}(OH)_2 \rightarrow 3MgSiO_3 + SiO_2 + H_2O$), as described by Moore and Reynolds (1997).

Between 1000°C and 1100°C, the recrystallization of metakaolinite and quartz occurs, forming mullite and cristobalite. At 1200°C, mullite and cristobalite become the dominant phases, while the enstatite formed recrystallizes into clinoenstatite, a high-temperature polymorph of $MgSiO_3$.

The gresification graph analysis, illustrated in Figure 9, reveals that the sintering of the S_{10} and C_{20} ceramic formulations becomes significant only at temperatures above 1000°C and 1050°C, respectively. At temperatures below these values, the formulations exhibit minimal linear firing shrinkage, high water absorption above 15%, and low flexural strength, as shown in Figure 10. This suggests that the material's microstructure remains porous and that particle cohesion is insufficient to provide the desired mechanical properties.

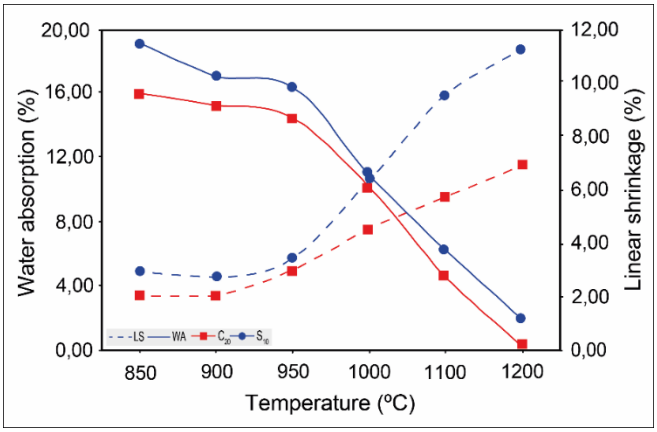

Figure 9 – Gresification curve of the C_{20} and S_{10} formulations.
Source: Authors (2024).

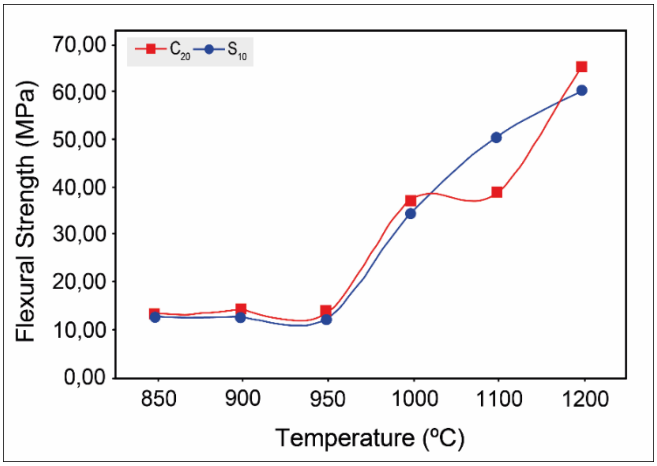

Figure 10 – Flexural strength as a function of temperature for the C_{20} and S_{10} formulations.
Source: Authors (2024).

The sintering of the S_{10} and C_{20} ceramic formulations exhibits a thermally activated behavior, with a significant increase in linear firing shrinkage at elevated temperatures. Specifically, the S_{10} formulation shows a notable increase in linear shrinkage from 1000°C, with values rising from 2.75% to 11.23% as the temperature reaches 1200°C. Meanwhile, the C_{20} formulation follows a similar pattern but starts later, with linear shrinkage increasing from 2.08% to 6.86% between 1050°C and 1200°C. This variation suggests that sample densification, through pore closure and liquid phase formation, is more pronounced at temperatures above 1000°C, especially in the S_{10} formulation, reflecting greater sintering efficiency.

The mechanical strength analysis of the S_{10} and C_{20} ceramic formulations, as presented in Figure 10, reveals a significant variation in values as a function of firing temperature. It is observed that for the S_{10} formulation, flexural strength ranges between 12.45 MPa and 60.39 MPa, indicating a substantial increase as the firing temperature rises, suggesting progressive material densification. Similarly, the C_{20} formulation exhibits strength variations between 12.60 MPa and 65.50 MPa, demonstrating analogous behavior but with slightly higher values at peak strength. These results indicate that both formulations respond positively to sintering, with improved mechanical properties as the firing temperature increases.

The apparent porosity data for the S_{10} and C_{20} ceramic formulations, presented in Figure 11, exhibit behavior similar to that observed for the water absorption parameter.

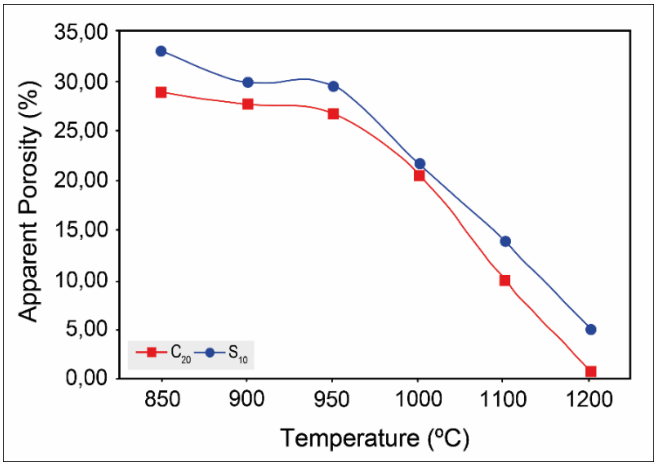

Figure 11 – Apparent porosity as a function of temperature for the C_{20} and S_{10} formulations. Source: Authors (2024).

Based on the results obtained from the flexural strength, linear firing shrinkage, apparent porosity, and water absorption tests, the C_{20} and S_{10} ceramic formulations exhibit characteristics that allow their application in the ceramic sector. The C_{20} formulation, upon reaching 1200°C, displays a water absorption of 0.29% and a flexural strength of 65.5 MPa, while the S_{10} formulation, at the same temperature, exhibits a water absorption of 1.99% and a flexural strength of 60.39 MPa. Although these results indicate properties close to those of materials used in ceramic coatings, additional criteria must be considered for classification according to technical standards. On the other hand, at lower temperatures, such as 850°C and 900°C, both formulations exhibit typical characteristics of red ceramics, such as high apparent porosity and water absorption above 15%, making them suitable for the production of ceramic blocks and bricks. This application aligns with the requirements established in the ABNT NBR 15310:2019 and ABNT NBR 15270-1:2017 standards, which regulate ceramic components for masonry and ceramic tiles, respectively.

Conclusions

The chemical and mineralogical analysis of the raw materials, as well as the behavior of the ceramic formulations at different firing temperatures, provided valuable insights into the potential of these compositions for industrial applications. The clay (A) demonstrated a composition rich in silicon oxide (SiO_2) and aluminum oxide (Al_2O_3), with low levels of fluxing oxides, indicating its suitability for the production of high-quality ceramic materials. In contrast, the emerald residues from the Carnaíba (C) and Socotó (S) mines exhibited a higher concentration of fluxing oxides, especially in the S samples, which favors the synthesis of mullite and other high-temperature phases, such as indialite.

The physical behavior of the ceramic pieces was evaluated through linear shrinkage and water absorption tests. The results revealed that as the firing temperature increases, progressive sintering of the pieces occurs, resulting in greater shrinkage and lower water absorption, particularly in the C and S formulations with emerald residue contents between 10% and 20%. This sintering process is facilitated by the formation of a liquid phase, which promotes dense particle packing and reduces porosity.

The flexural strength tests indicated that the formulations containing emerald residue exhibited acceptable thermal and mechanical performance, especially above 1000°C, when the formation of mullite and other phases contributed to increased mechanical strength. However, a slight tendency for strength reduction at 1100°C was observed in the C and S formulations with residue contents between 30% and 50%. This may be related to the thermal expansion of micas and the formation of internal cracks due to the structural transformation of quartz.

At high temperatures, around 1200°C, the C_{20} formulation stood out for exhibiting excellent thermal stability, sintering, and mechanical strength, making it particularly suitable for applications in the ceramic sector, such as coatings and flooring, which require high durability and low water absorption. The S_{10} formulation, in turn, proved to be promising for the production of advanced ceramic materials, with potential applications in the civil industrial sector due to its ability to form phases such as mullite and indialite, which provide high mechanical strength and superior thermal stability essential characteristics for structural materials and high-performance coatings.

Furthermore, the C_{20} and S_{10} formulations demonstrated considerable potential for use in the red ceramics sector. At lower temperatures, such as 850°C and 900°C, both formulations exhibited high apparent porosity and water absorption above 15%, properties typical of materials used in the production of ceramic blocks and bricks, according to the criteria established in the ABNT NBR 15310:2019 and ABNT NBR 15270-1:2017 standards. Thus, the C_{20} and S_{10} formulations present potential applications in different segments of the ceramic industry, ranging from ceramic coatings provided that additional tests are conducted to confirm their suitability to red ceramic products at lower firing temperatures.

It is therefore concluded that the incorporation of emerald residue from the Carnaíba and Socotó mines in proportions of 10% to 20% in ceramic formulations is the most suitable for achieving the desired physical and mechanical properties. On the other hand, residue contents above 20% require further studies to optimize formulation performance. This study has significantly contributed to the development of a sustainable solution for the utilization of emerald residue, a material that currently has a negative environmental impact.

Acknowledgments

We thank the Graduate Program in Geology at UFC for its support and financial assistance in conducting field activities. We also extend our gratitude to the Centro Regional para o Desenvolvimento Tecnológico e Inovação (CRTI) for carrying out the analyses; to the AEEP research group at IFBA for technical support; and to the Laboratórios de Degradação e Estabilização e Compostos (LabDEC) and Ensaios Mecânicos da Universidade de Brasília (UnB) for their support in the development of technological tests.

References

Acevedo, N. I. A.; Rocha, M. C. G.; Bertolino, L. C. Mineralogical characterization of natural clays from Brazilian Southeast region for industrial applications. *Cerâmica*, v. 63, n. 366, 253-262, 2017. Disponível em: https://www.researchgate.net/publication/317133042. Acesso em: 26 ago. 2024.

ABNT NBR 13818. *Argamassa para assentamento e revestimento de paredes e tetos – Requisitos.* Rio de Janeiro: Associação Brasileira de Normas Técnicas, 2017.

ABNT NBR 15270-1. *Componentes cerâmicos – Blocos e tijolos para alvenaria – Parte 1: Requisitos*. Rio de Janeiro: Associação Brasileira de Normas Técnicas, 2017.

ABNT NBR 15310. *Amostras de solo – Preparação para ensaios de compactação e ensaios de caracterização*. Rio de Janeiro: Associação Brasileira de Normas Técnicas, 2019.

Babisk, M.P.; Vidal, F. W. H.; Ribeiro, W. S.; Aguiar, M. C.; Gadioli, M. C. B.; Vieira, C. M. F. Incorporation of quartzite waste in red ceramic. *HOLOS*, v. 28, n. 6, 169-177, 2012.

Braga, P. F. A. *Caracterização e beneficiamento da molibdenita da região de Campo Formoso – BA*. São Paulo, 2013. 147f. Tese (Doutorado em Engenharia Metalúrgica) – Escola Politécnica, Universidade de São Paulo, São Paulo, 2013. Disponível em: https://doi.org/10.11606/T.3.2013.tde-26062014-215632. Acesso em: 26 ago. 2024.

Burch, R. Preparation of high surface area reduced molybdenum oxide catalyst. *Journal of the Chemical Society, Faraday Transactions 1*: Physical Chemistry in Condensed Phases, v. 74, 2982-2990, 1978. Disponível em: https://doi.org/10.1039/F19787402982. Acesso em: 26 ago. 2024.

Cavalcante, R. F. *Estudo do potencial de utilização do resíduo da extração de esmeraldas na fabricação de cerâmica de revestimento*. Natal, 2010. 103f. Dissertação (Mestrado em Engenharia Mecânica), Universidade Federal do Rio Grande do Norte, Natal, 2010.

Cavalcante, R. F.; Nascimento, R. M.; Paskocimas, C. A.; Dutra, R. P. S. 2012. Utilização do resíduo da extração de esmeraldas em uma formulação de massa de revestimento cerâmico. *Cerâmica*, v. 58, 158-164. 2012.

Irvine, J. T. S.; Murphy, R. J. *Ceramic materials*: Science and engineering. Springer, 2018. 766p.

Kang, S. J. L. *Sintering*: Densification, Grain Growth and Microstructure. Elsevier Butterworth-Heinemann, 2004. Disponível em: https://www.researchgate.net/publication/259781835. Acesso em: 26 ago. 2024.

Kumar, M.; Patel, A. *Modern ceramic engineering*: Advances in processing, characterization, and applications. CRC Press, 2022. 534p.

Lima, P. T.; Bertran, C. A.; Thim, G. P. Rotas de síntese e a homogeneidade dos precursores de mulita e cordierita. *Química Nova*, v. 21, n. 5, 553-562, 1998.

Macedo, R. S.; Menezes, G. A.; Neves, G. de A.; Ferreira, H. C. Estudo de argilas usadas em cerâmica vermelha. *Cerâmica*, v. 54, n. 332, 411-417, 2008. Disponível em: http://dx.doi.org/10.1590/S0366-69132008000400005. Acesso em: 26 ago. 2024.

Marschner, H. F. *Mineralogy*. 2. ed. New York: Springer, 2011.

Menezes, R. R.; Campos, L. F.; Neves, G. de A.; Ferreira, H. C. Estudo sobre as propriedades de cerâmicas vermelhas incorporadas com resíduos de quartzito. *Cerâmica*, v. 52, 2006.

Menshaz, A. M.; Johari, M. A. M.; Ahmad, Z. A. Characterization of metakaolin treated at different calcination temperatures. *AIP Conference Proceeding*, v. 1892, n. 1, 2017. Disponível em: https://www.researchgate.net/publication/320445890. Acesso em: 26 ago. 2024.

Moore, D. M.; Reynolds, R. C. Jr. *X-ray diffraction and the identification and analysis of clay minerals.* 2. ed. Oxford: Oxford University Press, 1997. 352p.

Moreno, M. M. T.; Del Roveri, C.; Godoy, L. H.; Zanardo, A. Caracterização de argilas e composição de massas cerâmicas preparadas com base na análise de curvas de consistência de misturas argila-água. *Cerâmica*, v. 62, n. 361, 21-31, 2016. Disponível em: https://www.scielo.br/j/ce/a/XDzdpvWBcmH7LcMY8bSM9nm/. Acesso em: 26 ago. 2024.

Prado, C. M. O. *Caracterização Química e Mineralógica das Argilas Utilizadas na Produção de Cerâmica Vermelha no Estado de Sergipe*. São Cristóvão, 2011. 82f. Dissertação (Mestrado em Geologia) – Universidade Federal de Sergipe, São Cristóvão, 2011. Disponível em: https://ri.ufs.br/handle/riufs/6126. Acesso em: 26 ago. 2024.

Santos, P. S. *Ciência e Tecnologia de Argilas*. v. 1, 2. ed. São Paulo: Editora Edgard Blücher Ltda, 1989. 802p.

Santos, S. C. A.; Torres, P. W. T. S.; Mercury, J. M. R.; Angélica, R. S.; Neves, R. F. Estudo cinético do processo de desidroxilação da caulinita. *In*: 57º Congresso Brasileiro de Cerâmica, 2013, Natal. Anais... ABCERAM, 2013. 1775-1787.

Schroeder, K.; Kalidindi, S. R. *High-performance ceramic materials*: Advances in processing and applications. Wiley, 2023.

Silveira, M. D. *Utilização de resíduos de mineração na construção civil*. Belo Horizonte, 2015. 39f. Monografia (Especialização em Construção Civil), Departamento de Engenharia de Materiais e Construção Civil, Universidade Federal de Minas Gerais, Belo Horizonte, 2015.

Sokhanvar, S.; Sadeghi, M. *Advances in ceramics: synthesis, processing, and applications*. Oxford: Elsevier, 2020. 534p.

Vieira, C. M. F.; Dias, C. A. C.; Mothé, A. V.; Sanchez, R.; Monteiro, S. N. Incorporação de lama de alto forno em cerâmica vermelha. *Cerâmica*, v. 53, 381-387, 2007. Disponível em: https://www.researchgate.net/publication/240971747. Acesso em: 26 ago. 2024.

Yin, Q.; Zhu, B.; Zeng, H. *Microstructure, property and processing of functional ceramics*. Berlin, Heidelberg: Springer, 2010. 400p.